Supporting information

Unraveling the Mechanism for H_2O_2 Photogeneration on Polymeric Carbon Nitride with Alkali Metal Modification

Zehao Li [1,2,*] and Yufei Chen [2]

[1] Guangdong Provincial Key Laboratory of Chemical Measurement and Emergency Test Technology, Institute of Analysis, Guangdong Academy of Sciences (China National Analytical Center, Guangzhou), Guangzhou 510070, China
[2] School of Chemistry and Chemical Engineering, Anyang Normal University, Anyang 455000, China
* Correspondence: zehaoli512@outlook.com

Experimental Section

Characterization

To analyze the structure of PCN, X-ray diffraction (XRD, Rigaku Corporation Ultima III), Fourier transform infrared spectroscopy (FT–IR, Thermo Scientific Nicolet iS50ATR), X-ray photoelectron spectroscopy (XPS, Thermo Scientific K-Alpha^{+}), and solid-state ^{13}C nuclear magnetic resonance spectroscopy (NMR, Bruker Advance III 500 spectrometer) were performed. The morphology and specific surface area of obtained PCN were characterized via scanning electron microscopy (SEM, Hitachi SU8010) and the Brunauer–Emmett–Teller (BET) (Micrometrics Gemini VII 2390) analyses, respectively. The optical absorption properties and charge recombination of obtained PCN were measured via ultraviolet–visible (UV–Vis, Shimadzu UV-2550 UV-vis spectrophotometer) and photoluminescence (PL, Edinburgh FLS980 spectrometer) spectroscopies (under excitation at 370 nm), respectively. The carrier lifetimes were determined at room temperature employing time-resolved PL (Edinburgh FLS980 spectrometer). The adsorptions of NH_3 and O_2 on catalysts were measured via temperature-programmed desorption (TPD) using a chemisorption analyzer (Chembet TPR/TPD Micromeritics 2920).

Photoelectrochemical measurement

The measurement of the rotating disk electrode (RDE, Pine Co., Ltd) was conducted employing a three-electrode cell on a CHI 660E system. The linear sweep voltammetry (LSV) was detected in 0.1 M phosphate buffer solution (PBS, pH=7, O_2-saturated) with the scan rate of 5 mV/s. And the rotating speed of the working electrode was 400 rpm, 900 rpm, 1600 rpm and 2500 rpm, respectively. The transfer electron number (n) of O_2 reduction was calculated by the slopes of Koutecky-Levich plots with following equation:

$$j^{-1} = j_k^{-1} + B^{-1}\omega^{-1/2} \qquad \text{(S1)}$$

$$\mathrm{B} = 0.2\mathrm{nF}C_0 D_0^{2/3} v^{-1/6} \qquad \text{(S2)}$$

j is current density (mA/cm^2); j_k is the kinetic current density; ω is the angular velocity (rpm); F is Faraday constant (96485 C/mol); C_0 and D_0 are bulk

concentration of O_2 (1.1×10^{-3} mol/cm^{-3}) and diffusion coefficient of O_2 (1.93×10^{-5} cm^2/s), respectively; v is dynamic viscosity of H_2O (0.01 cm^2/s).

Electrochemical impedance spectroscopy (EIS), the periodic on/off photocurrent response, and the Mott–Schottky plots were tested on an electrochemical workstation (Chenhua CHI 660E, Shanghai) employing a conventional three-electrode system.

Density functional theory (DFT) calculations

All the calculations based on density functional theory (DFT) were performed by using the Vienna Ab initio Simulation Package (VASP) [1-2]. The exchange–correlation effects were described by the generalized gradient approximation (GGA)[3] combined with the Perdew-Burke-Ernzerhof (PBE)[4]. The interactions between cores and valence electrons were treated using the projector augmented wave (PAW)[5]. During the calculations, the plane-wave cut off energy of 400 eV was used, and the Monkhorst-Pack Γ-centered grid of 1×1×1 was used for all structure optimization. The convergence thresholds of 10^{-5} eV and 0.02 eV/Å were employed for energy and force, respectively. A large vacuum space of 15 Å was sed to avoid the effects from the periodic boundary conditions.

The adsorption energies ΔE_{ads} were calculated from the following formula:

$$\Delta E_{ads} = E_{substrate-O_2/C_2H_5OH} - E_{substate} - E_{O_2/C_2H_5OH}$$

Where $E_{substrate-O_2/C_2H_5OH}$ and $E_{substate}$ are the total energies of substrate-O_2/C_2H_5OH composites and the substrate, respectively. E_{O_2/C_2H_5OH} is the energy of the isolated O_2/C_2H_5OH.

Dissolved oxygen (DO)

The dissolved oxygen concentration in the solution was tested by dissolved oxygen meter (Shanghai Yoke Instrument Limited Company, L-512). First, the DO value in the ethanol solution was tested. And then the catalyst was added into the solution. After stirring for 30 min under dark conditions, the DO in the reaction solution was tested. Then the white LED light was turned on immediately. The photocatalytic process was performed for 1 h at a 15-min interval for the DO testing.

Results Section

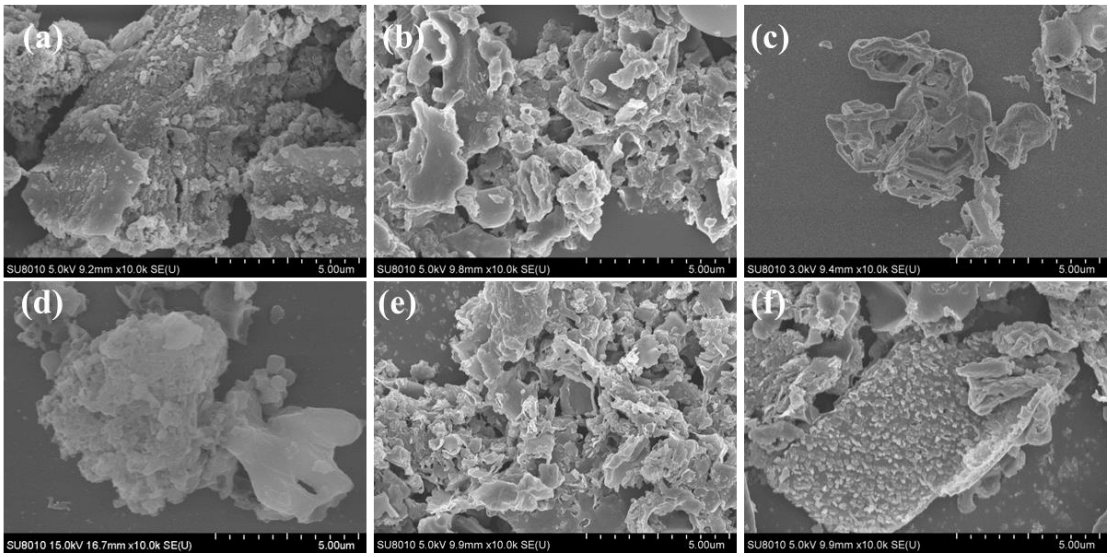

Figure S1. SEM images of obtained PCN: (**a**) CN, (**b**) CN-Li, (**c**) CN-Na, (**d**) CN-K, (**e**) CN-Rb, (**f**) CN-Cs.

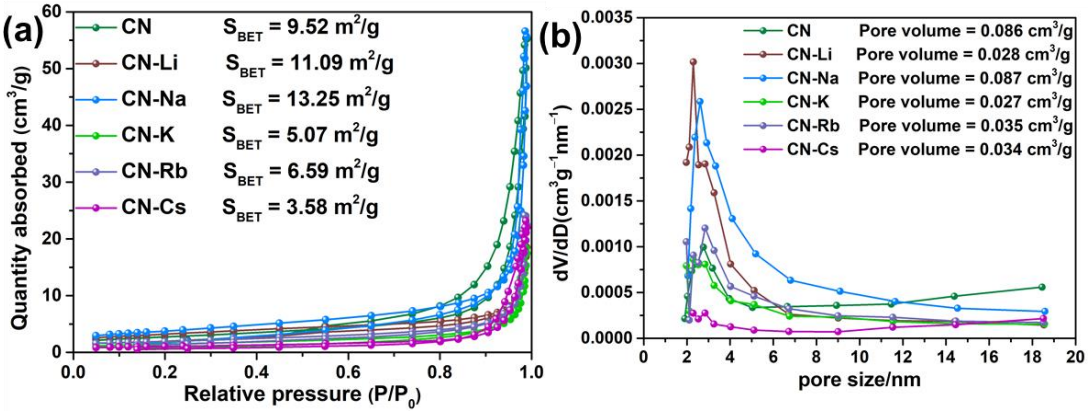

Figure S2. (**a**) N_2 adsorption-desorption isotherms. (**b**) the pore size distribution curves of the obtained PCN.

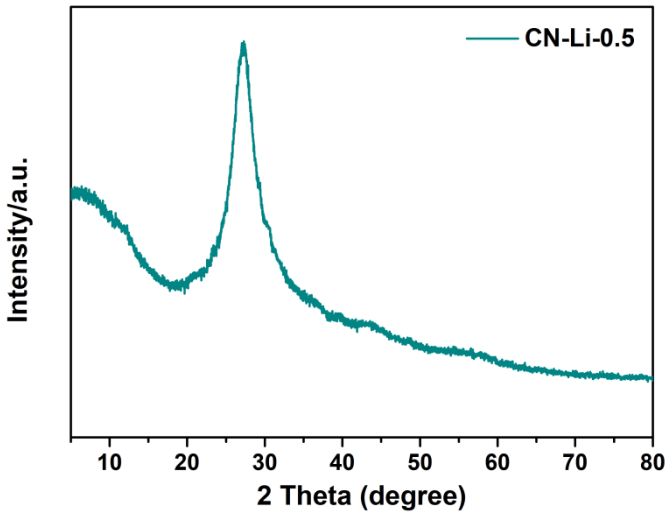

Figure S3. XRD pattern of CN-Li-0.5 (the added amount of LiCl is 0.5 g).

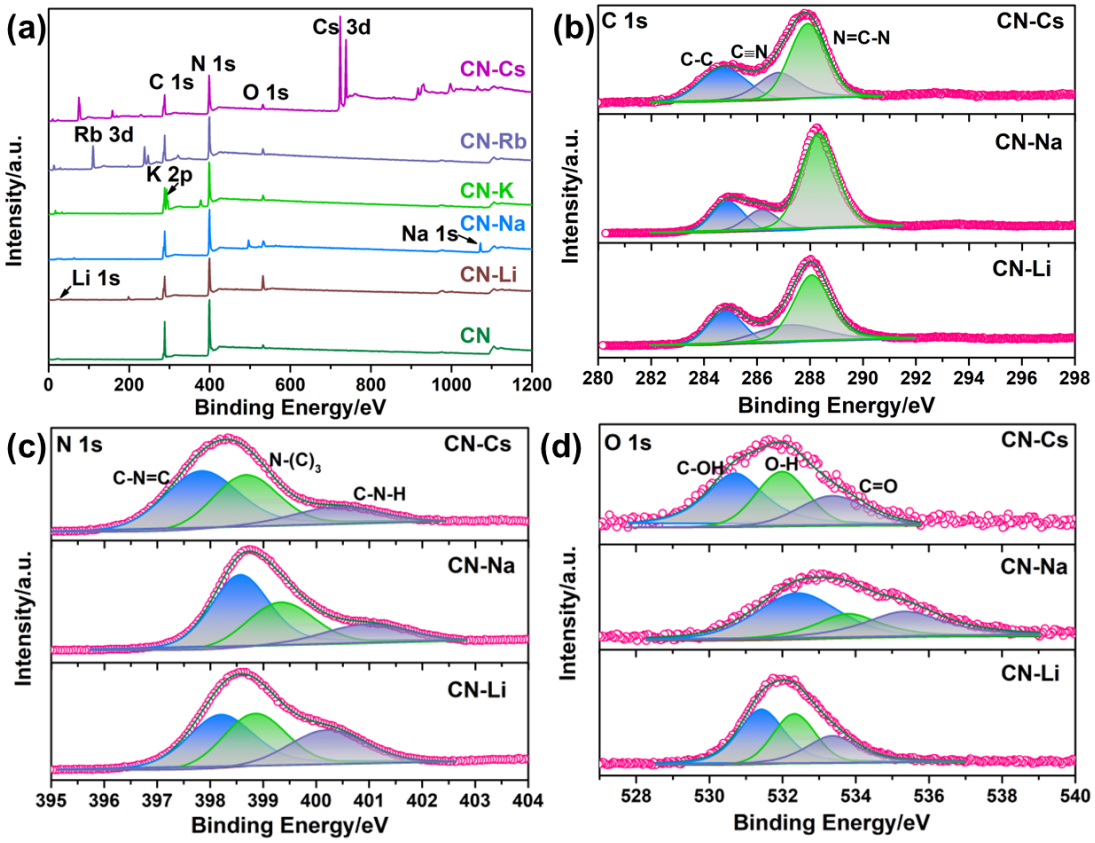

Figure S4. (**a**) XPS survey of obtained PCN. (**b**) High-resolution XPS spectra of C 1*s* of obtained PCN. (**c**) High-resolution XPS spectra of N 1*s* of obtained PCN. (**d**) High-resolution XPS spectra of O 1*s* of obtained PCN.

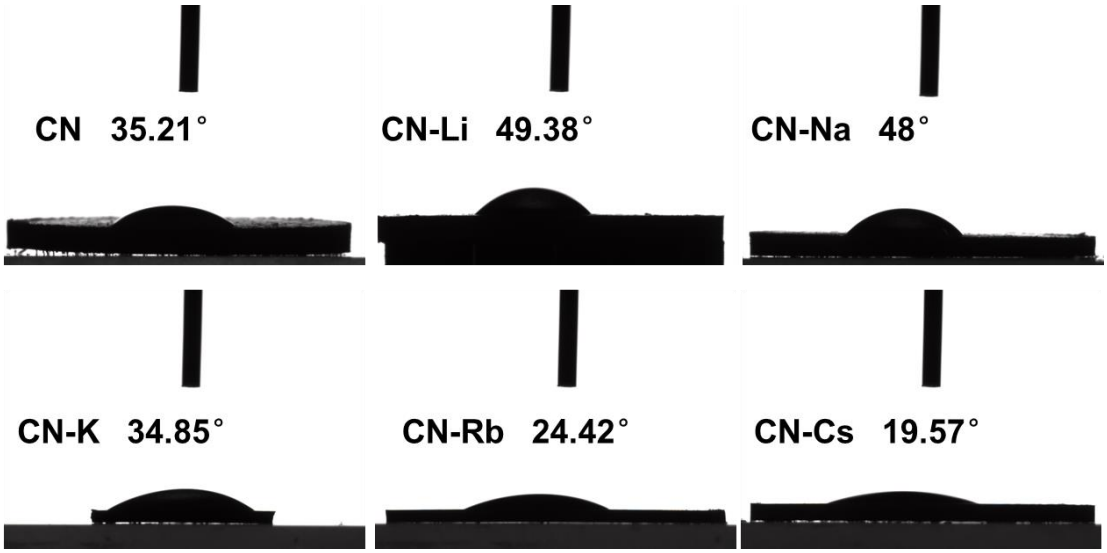

Figure S5. Digital images of contact angle tests for PCN.

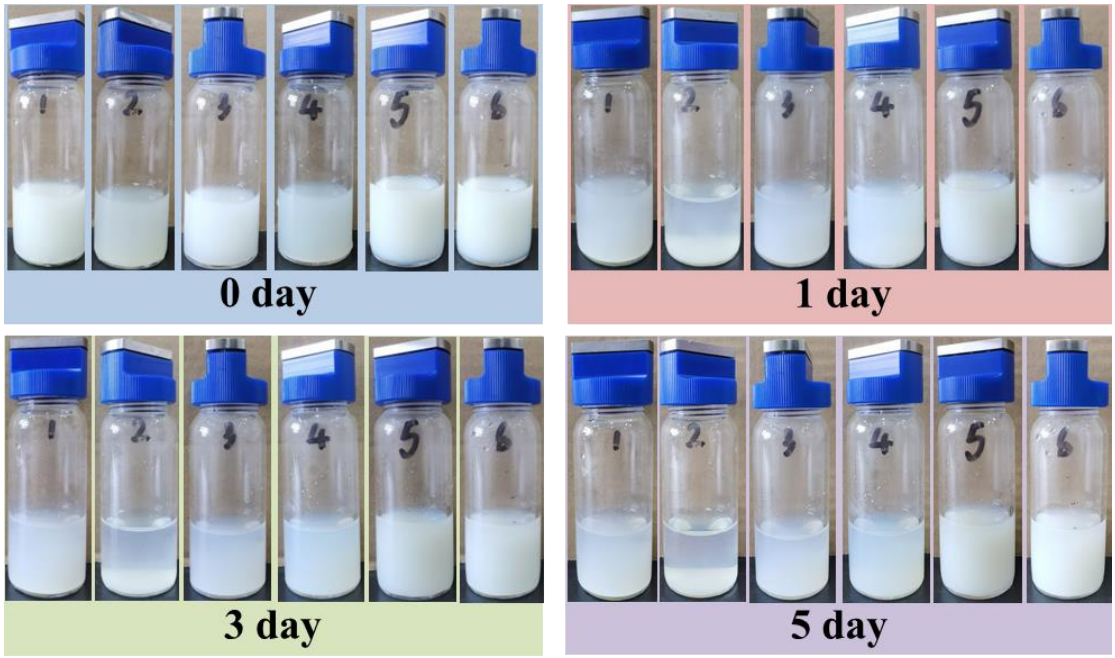

Figure S6. The photographs of CN and CN-M dispersed in deionized water for 7 days.

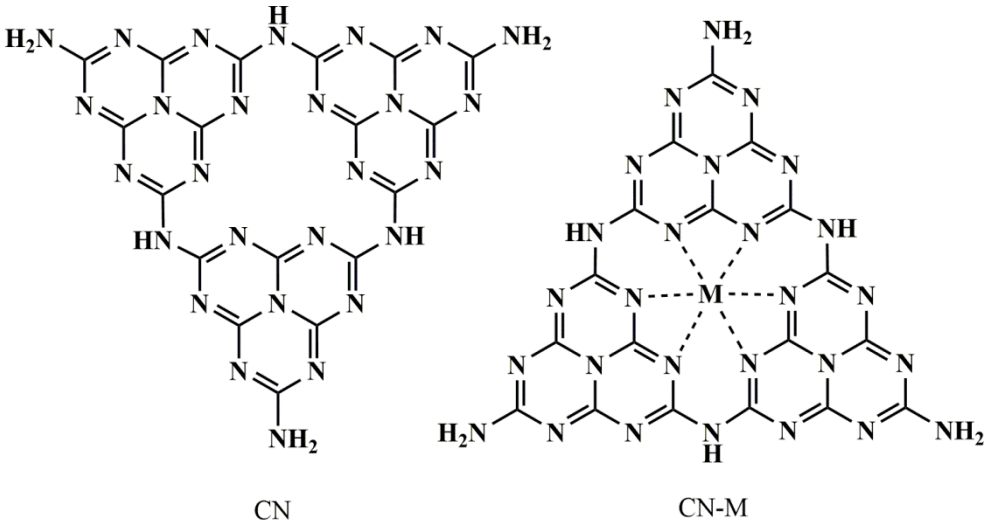

Figure S7. The chemical structures of CN and CN-M.

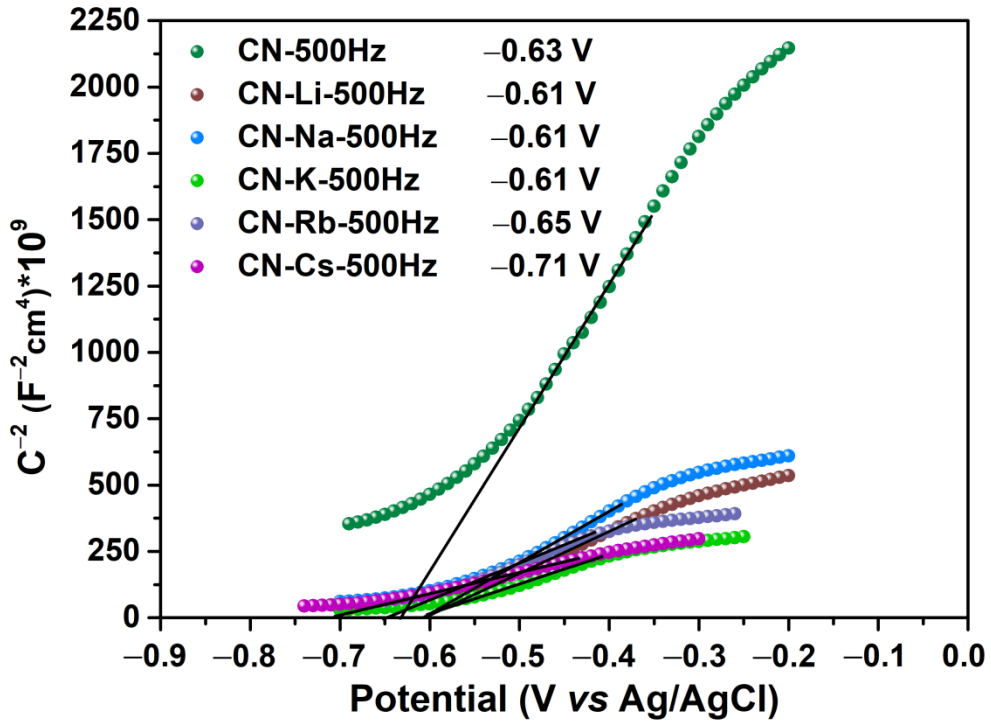

Figure S8. Mott–Schottky plots over 500 Hz in 0.5 M Na_2SO_4 and 0.2 M phosphate buffer electrolyte.

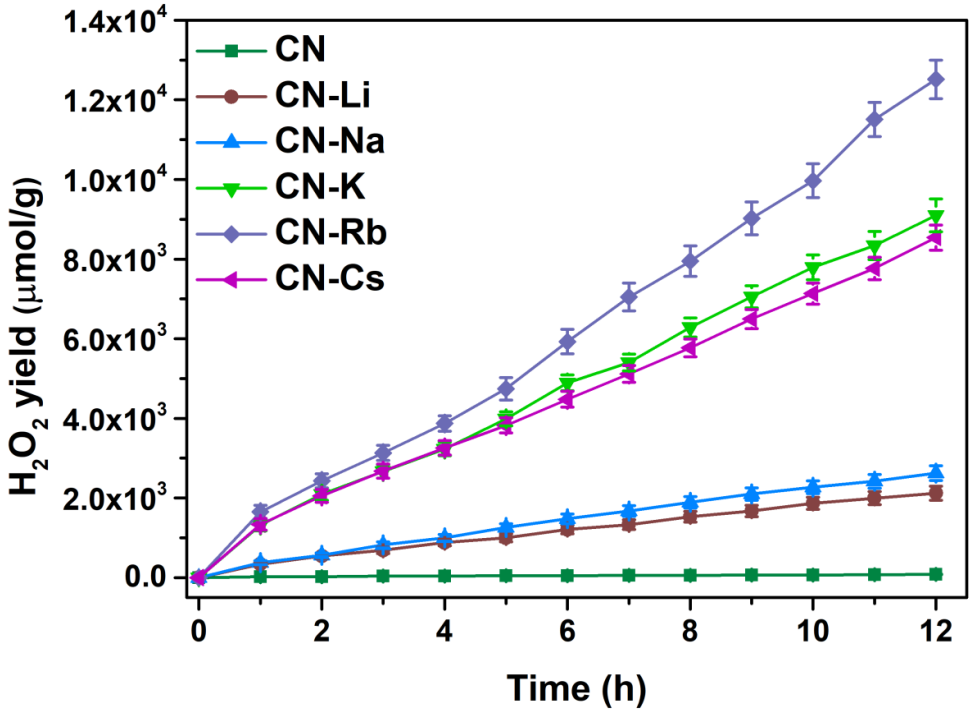

Figure S9. Time-dependent change in H_2O_2 evolution during photoreaction with PCN under visible light (λ > 420 nm).

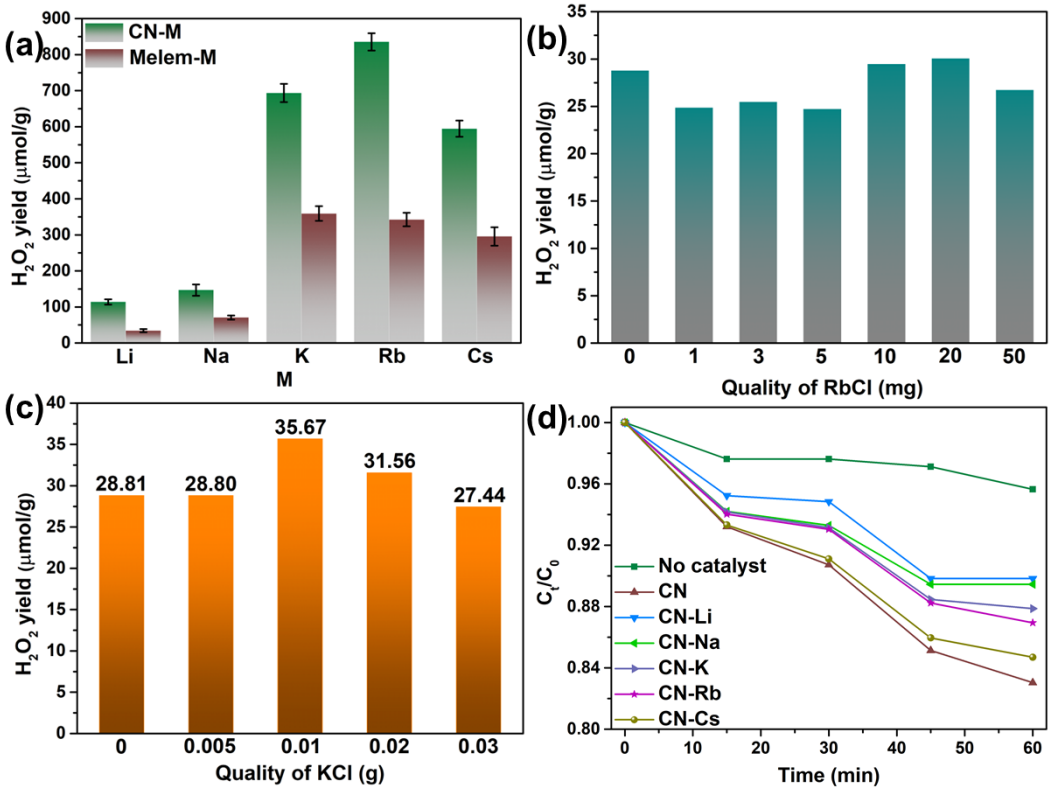

Figure S10. (**a**) The photocatalytic H_2O_2 production of modified PCN with different methods. (**b**) The photocatalytic H_2O_2 production of CN with different amount of

RbCl. (**c**) The photocatalytic H_2O_2 production of CN with different amount of KCl. (**d**) The photocatalytic decomposition of H_2O_2 for CN and CN-M under LED white light. The initial concentration of H_2O_2 is 1 mM. And the detailed operation is that 0.01 g of the photocatalyst is adequately dispersed in 50 mL distilled water. After bubbling N_2 for 5 min, turn on LED light. The photocatalytic decomposition is performed for 1 h with a 15-min interval for sample collection. The H_2O_2 concentration was determined by the colorimetric method, which is based on the peroxidase (POD)-catalyzed oxidation of N, N-diethyl-*p*-phenylenediamine (DPD) by hydrogen peroxide.

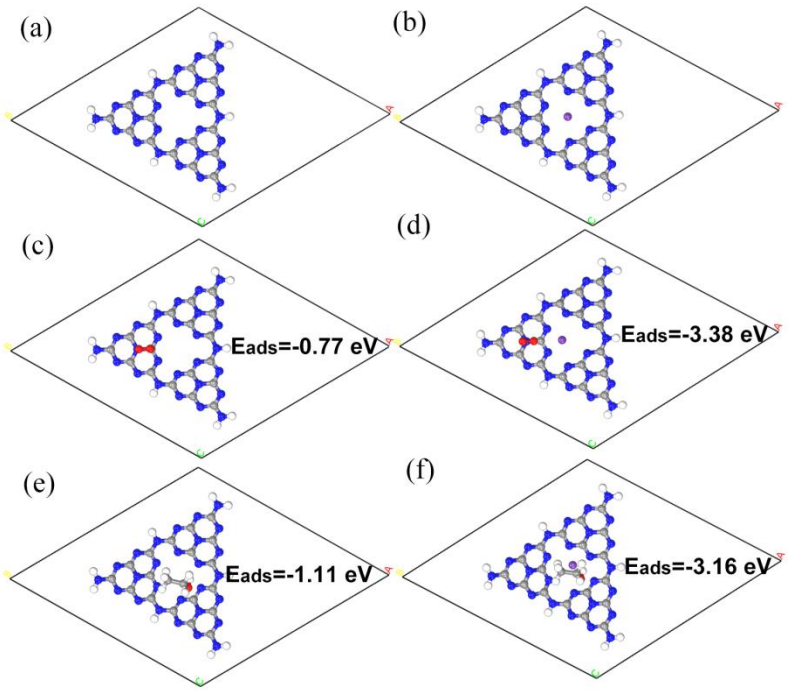

Figure S11. The DFT calculations for CN and CN-Rb. Polymeric models for CN (**a**) and CN-Rb (**b**); The adsorption energies onto CN (**c**) and CN-Rb (**d**) for oxygen; The adsorption energies onto CN (**e**) and CN-Rb (**f**) for ethanol.

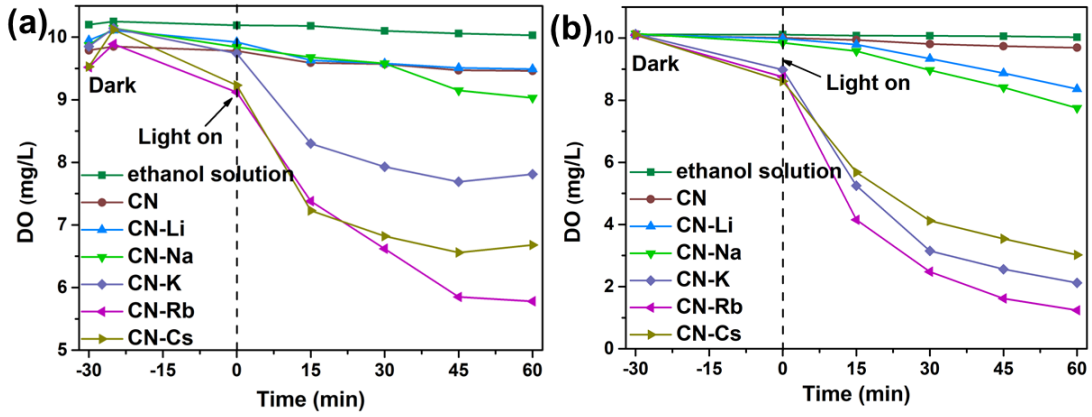

Figure S12. The dissolved oxygen (DO) concentrations of reaction solution for the obtained PCN and without catalyst. (**a**) open system; (**b**) closed system with catalyst degassing treatment. Namely, 0.03 g catalyst is placed in a vacuum drying oven for degassing. The degassed catalyst is added into 50 mL ethanol aqueous solution quickly. Then the reaction bottle is sealed, and there is no air above the solution (as shown in Figure S14).

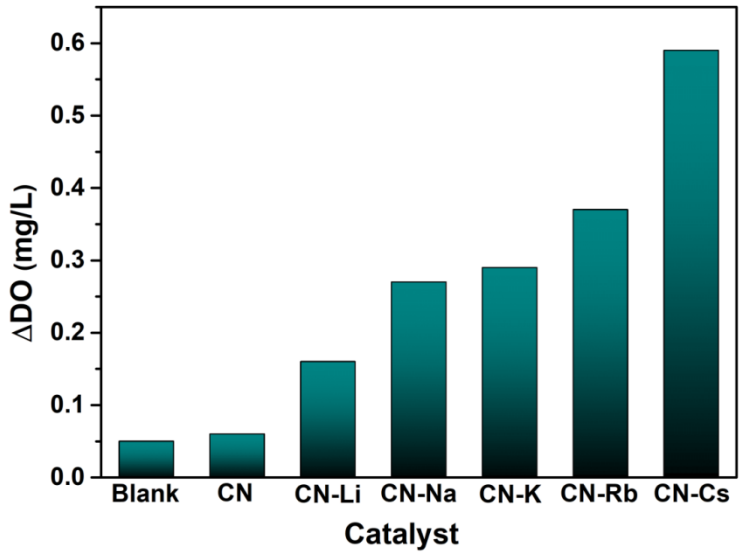

Figure S13. The D-value of the initial DO and the DO after stirring 5 min for the obtained PCN.

Figure S14. The DO test device with closed system.

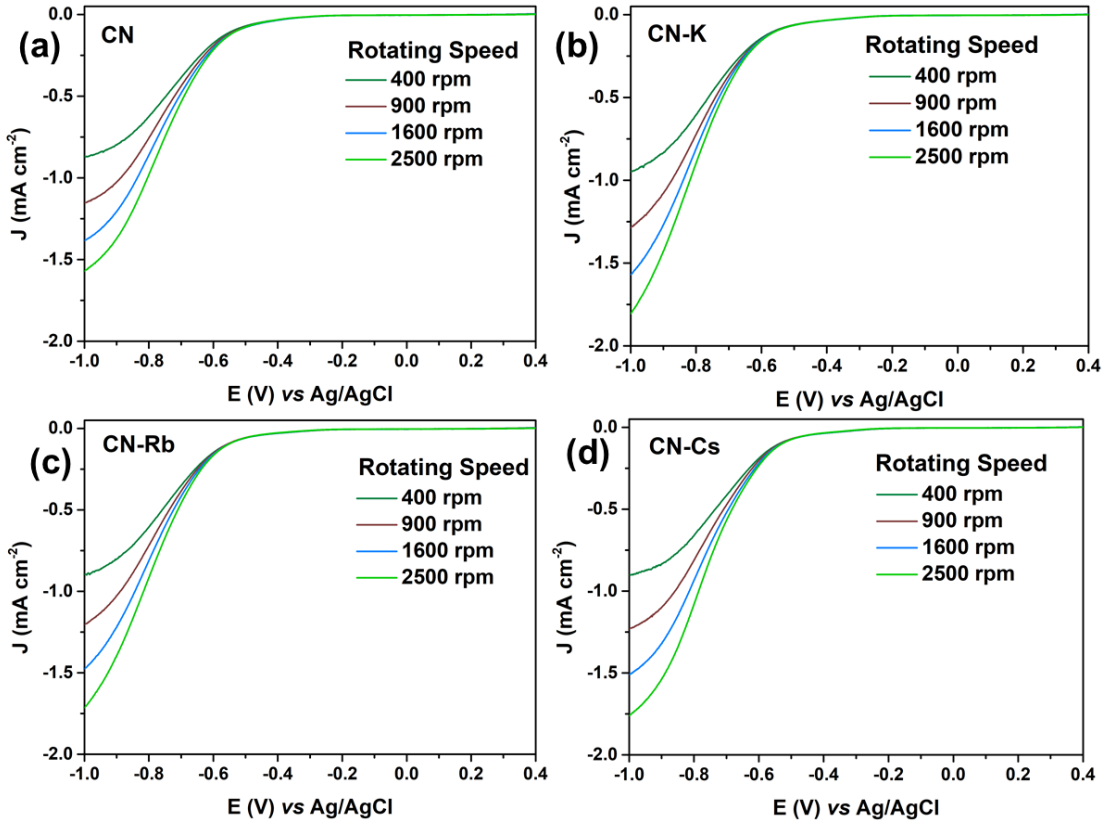

Figure S15. LSV curves of (**a**) CN, (**b**) CN-K, (**c**) CN-Rb, and (**d**) CN-Cs were measured on an RDE at different rotating speeds.

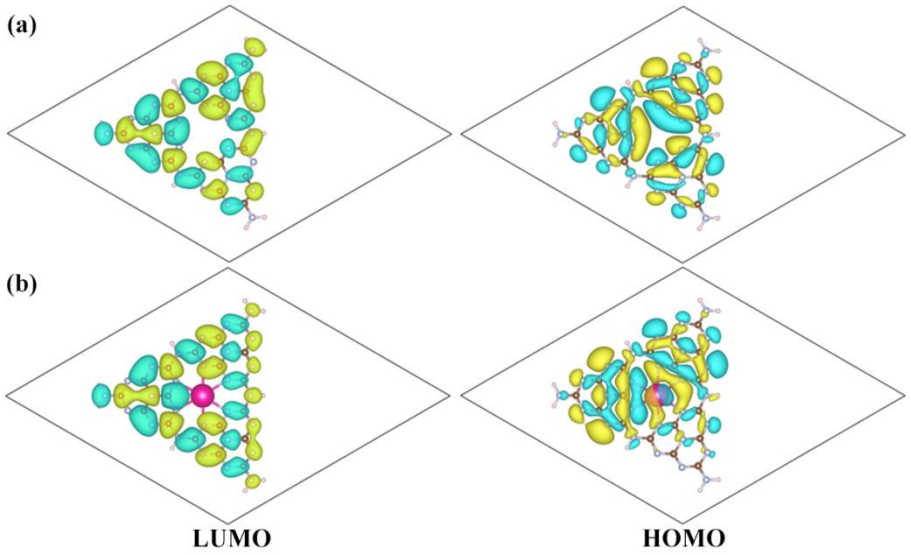

Figure S16. Electronic structures of polymeric models for (**a**) CN and (**b**) CN-Rb together with their optimized HOMO and LUMO.

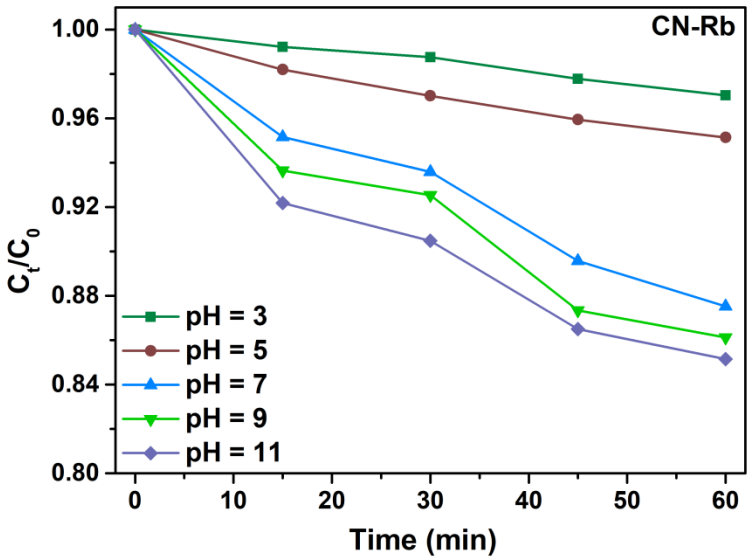

Figure S17. The effect of solution pH on the decomposition of H_2O_2 for CN-Rb under LED white light.

Table S1. Physicochemical properties of the as-prepared samples.

Sample	addition of M (g)	S_{BET} (m^2/g)	Band-gap (eV)	τ (ns)	it (μA/cm^2)
CN	/	9.52	2.74	2.10	0.25
CN-Li	1.1	11.09	2.57	2.39	0.29
CN-Na	0.5	13.25	2.70	2.38	0.55
CN-K	0.5	5.07	2.68	6.82	0.74
CN-Rb	0.5	6.59	2.68	17.95	1.76
CN-Cs	0.5	3.58	2.68	2.88	0.43

Table S2. XPS peak area ratio of the as-prepared samples.

Sample	CN	CN-Li	CN-Na	CN-K	CN-Rb	CN-Cs
C–N=C	49.18%	40.99%	53.46%	49.46%	48.13%	50.28%
N–$(C)_3$	31.76%	33.69%	31.15%	38.48%	37.16%	36.00%
C–N–H	19.06%	25.32%	15.39%	12.06%	14.71%	13.72%
C–C	13.36%	22.49%	17.76%	17.30%	18.95%	27.11%
C≡N	-	22.98%	14.45%	33.81%	17.84%	23.24%
N=C–N	86.64%	54.53%	67.79%	48.89%	63.21%	49.65%
C	41.67%	41.83%	47.78%	57.78%	54.98%	37.51%
N	56.14%	36.27%	41.00%	26.76%	35.38%	46.83%
O	2.20%	12.39%	7.84%	7.20%	7.21%	2.99%
Cl	-	0.65%	0.08%	0.09%	0.07%	0.21%
M	-	8.86%	3.30%	8.17%	2.36%	12.45%

Table S3. TPD values of obtained PCN.

Sample	NH_3 mmol/g	O_2 μmol/g
CN	0.38	13.18
CN-Li	0.40	35.48
CN-Na	0.41	43.47
CN-K	0.58	47.96
CN-Rb	0.72	97.47
CN-Cs	1.35	112.47

References:

1. Kresse, G.; Furthmüller, J. Efficiency of ab-initio total energy calculations for metals and semiconductors using a plane-wave basis set. *Comput. Mater. Sci.* **1996**, *6*, 15–50, https://doi.org/10.1016/0927-0256(96)00008-0.
2. Kresse, G.; Furthmüller, J., Efficient iterative schemes for ab initio total-energy calculations using a plane-wave basis set. Phys. Rev. B 1996, 54, 11169-11186.
3. Perdew, J.P.; Burke, K.; Ernzerhof, M. Generalized gradient approximation made simple. *Phys. Rev. Lett.* **1996**, *77*, 3865. https://doi.org/10.1103/PhysRevLett.77.3865.
4. Perdew, J.P.; Ernzerhof, M.; Burke, K. Rationale for mixing exact exchange with density functional approximations. *J. Chem. Phys.* **1996**, *105*, 9982–9985. htttps://doi:10.1063/1.472933
5. Kresse, G.; Joubert, D. From ultrasoft pseudopotentials to the projector augmented-wave method. *Phys. Rev. B* **1999**, *59*, 1758–1775. https://doi.org/10.1103/physrevb.59.1758.